FUNCTIONAL STUDY OF A DISTRIBUTED MPPT POWER MANAGEMENT SYSTEM

S. Bifaretti [(1)], S. Pipolo [(1)], T. F. Catalano [(2)], G. Daprati [(2)], V. Iacovone [(2)], E. Scione [(2)]

[(1)] Department of Industrial Engineering, University of Rome Tor Vergata,Via del Politecnico 1 Rome, Italy
bifaretti@ing.uniroma2.it
[(2)] Thales Alenia Space Italia S.p.A., Via Saccomuro 24, Rome, Italy, { toni.catalano, giorgio.daprati, vincenzo.iacovone, emiliano.scione, }@thalesaleniaspace.com

ABSTRACT

This paper presents the concept of a control strategy for Solar Array (SA) power regulation using an independent Maximum Power Point Tracking system for each Solar Array section in order to maximize the power extracted from every SA sections. Moreover, it allows to distribute the battery charge current between the power sources in order to evenly divide the switching losses on the power semiconductors of the converters and, thus, extending their life time and to reduce the dissipation power. The proposed strategy can be applied to the Power Control Unit designed for satellites with unregulated power bus architecture. Significant simulation results, obtained using a Matlab/Simulink model, demonstrates the validity of the proposed approach.

1. INTRODUCTION

Solar Array (SA) regulation systems based on Maximum Power Point Tracking (MPPT) have been largely developed and implemented for spacecraft applications in the last years. The architectures related to MPPT systems can be classified, as illustrated in [1], in parallel [2]-[4] or sectional [5]-[6]. In the first solution only one MPPT is used to achieve the voltage reference for the entire SA control. Such approach is valid in case the SA panels or wings are exposed to the same environmental conditions (e.g. temperature, illumination) and aging. However, these are ideal cases because both operational constraints (loss of sun pointing due to payload imaging manoeuvres) and standard entry/exit eclipse situations, imply different thermal and illumination conditions for the SA panels. On the contrary, sectional architectures, which employ separate MPPTs able to perform an individual tracking for each SA section, are preferred due to their better performances in extracting power from the sources. For this reason, the latter is accounted and discussed in this paper. Usually the references for the SA regulators are provided alternatively by the MPPT or by the output of the battery charge control loop on the base of the required load and battery power. The paper proposes a control scheme that employs, at the same time, a combination of both references in order to generate a proper control signal to the buck DC-DC converters chosen for SA regulation. The control method is applied to each converter using two different control loops in order to regulate at the same time the SA and the output currents.

2. SINGLE SECTION CONTROL

The control system, referred to a single section of the SA, combines a classical Perturb & Observe (P&O) MPPT algorithm with a battery charging regulation system, as shown in Fig. 1.

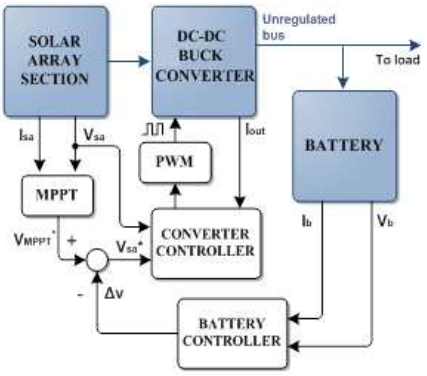

Figure 1: Block diagram of a single SA section.

The voltage reference V_{sa}^{*} for the buck converter is determined by the difference of V_{MPPT}^{*} and the output of the battery controller $\Delta v \leq 0$ so that the power balance between the SA, the load and the battery is satisfied.
The charging control of the battery is performed according to the Constant Current - Constant Voltage (CC-CV) algorithm. Based on SA power generation, battery State Of Charge (SOC) and load condition, it is possible to distinguish two different operation modes:

a) Battery discharging mode ($P_{load} > P_{sa}$)

In this case the input voltage reference of the buck converter V_{sa}^{*} is completely determined by the control signal coming from the MPPT algorithm (e.g. Δv=0), allowing the SA to operate at maximum power.

b) Battery charging mode ($P_{load} < P_{sa}$)

In this case, the system allows the charge of the battery according to the CC-CV algorithm.
As the battery progressively reduces its power demand, Δv becomes more and more negative, so that the voltage operating point of the SA decreases until the condition $P_{load} = P_{sa}$ is satisfied.

2.1. DC-DC Converter Control Loop

The double control loop shown in Fig. 2 has been used to regulate the SA voltage V_{sa} and on the output current of the converter I_{out}.
The conduction interval of the Power MOSFET M_n is determined according to the difference between the voltage reference V_{out}^*, provided by the MPPT, and the output current V_{out}. A feed-forward term r, achieved by the battery and SA voltage ratio, is also added to obtain a faster transient response. The reference current I_{out}^* is the sum of two terms: the first one is the difference between the desired voltage V_{sa}^* and the SA voltage measure, whilst the second is obtained by the feed-forward term FF, which takes into account the current supplied by the SA and the voltage ratio r.
These feed-forward terms have been accounted in order to fasten the control and permit to the PI regulators to work in a reduced operating range.

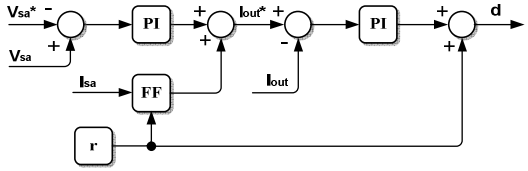

Figure 2: Single converter controller block diagram.

2.2. Battery Charge Control Loop

Fig. 3 shows the detailed block diagram of the battery controller, which is composed of two different control loops: the internal loop used for the battery constant current control, while the external loop employed for the constant voltage control.
The voltage loop sets the current reference at which the battery will recharge. The battery current limiter is used in order to set a maximum charging current level as long as the battery has not yet reached its maximum charged voltage command V_b^*, representing the End Of Charge Voltage (EOCV) value. In this case the system operates in the Constant Current (CC) charge mode. As the battery voltage reaches the EOCV, the controller switches in the Constant Voltage (CV) mode, so the charging current command I_b* progressively reduces to zero as soon as the battery is completely charged.
The battery current controller receives the battery charge current error at input and generates a positive limited control signal, namely Δv, that subtracted from the maximum power point reference V_{MPPT}^* determines the converter input voltage V_{SA}^*.

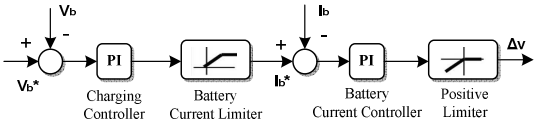

Figure 3. Battery controller block diagram.

3. POWER SYSTEM CONTROL

A SA composed of 4 sections has been considered. Each section is managed by independent MPPT and voltage controller and receives a control signal coming from the battery controller in order to select its appropriate operating point. The SA source can provide about 250W at Maximum Power Point (MPP) and End Of Life (EOL).
The power management proposed in this paper allows maximizing the power extracted from every SA sections. Moreover, it allows to distribute the battery charge current between the power sources in order to evenly divide the switching losses on the power semiconductors of the converters and, thus, extending their life time and to reduce the converter power dissipations. To this aim, as illustrated in Fig. 4, the battery controller provides 4 current error signals, each one proportional to the current supplied by the corresponding SA section. Then, each Δv_i (i=1..4) is calculated on the basis of the battery current error signal multiplied by the term 1-I_{sai}/I_{tot}, being I_{sai} the current supplied by i-th section and I_{tot} the total current supplied by all the SAs. Using such approach, each section provides a percentage of the battery current proportional to its own current, maximizing the current extraction from the sections providing the lowest power. On the other hand, this control logic resulted in a high robustness towards potential SA strings failures and variations of the operative conditions (both irradiance and temperature), allowing the system to operate correctly under different operative conditions, leading to an higher flexibility and to increase the system efficiency.

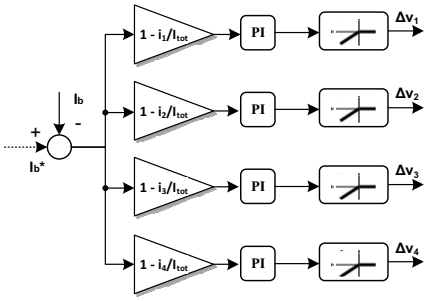

Figure 4: Modified battery controller block diagram.

4. SIMULATION MODELS

Simulations have been performed in Matlab/Simulink/ SimPowerSystem accounting an average model of the buck converter circuit, in order to highlight the performances of the controller independently from the power switching devices. Simulations consider an ideal behaviour of the electronic components.

4.1 Solar Array

Fig. 5 shows the single-diode equivalent circuit of a

Photovoltaic (PV) module whose physical parameters cannot be achieved directly from manufacturers datasheets. To overcome such a problem, in this paper the model of a PV module developed in [7] has been considered. Such a model, described later in detail, doesn't require the use of any complex numerical methods and employs only parameters provided by manufacturers' datasheets.

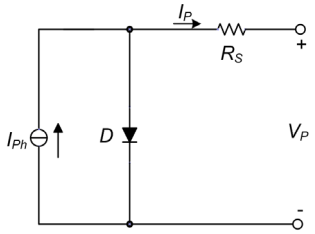

Figure 5: Equivalent circuit of a PV module.

The current of a PV module can be expressed, as function of voltage, by the simplified expression derived from [8]:

$$I_P = I_{SC} \cdot \left[1 - C_1 \cdot \left(e^{\left(\frac{V_P}{C_2 \cdot V_{OC}}\right)} - 1\right)\right] \quad (1)$$

where

$$C_1 = \left(1 - \frac{I_{MPP}}{I_{SC}}\right) \cdot e^{\left(\frac{-V_{MPP}}{C_2 \cdot V_{OC}}\right)} \quad (2)$$

$$C_2 = \frac{\left(\frac{V_{MPP}}{V_{OC}} - 1\right)}{\ln\left(1 - \frac{I_{MPP}}{I_{SC}}\right)} \quad (3)$$

Coefficients C_1 and C_2 depends on the following module parameters:

- short circuit current I_{SC};
- open circuit voltage V_{OC};
- maximum power point voltage V_{MPP};
- maximum power point current I_{MPP}.

Such parameters can be expressed as follow [7]:

$$I_{SC}(G,T) = I_{SCS}\frac{G}{G_S}[1 + \alpha(T - T_S)] \quad (4)$$

$$V_{OC}(G,T) = V_{OCS} + \beta(T - T_S) - \Delta V(G) \quad (5)$$

$$I_{MPP}(G,T) = I_{MPPS}\frac{G}{G_S}[1 + \alpha(T - T_S)] \quad (6)$$

$$V_{MPP}(G,T) = V_{MPPS} + \beta(T - T_S) - \Delta V(G) \quad (7)$$

where parameters I_{SCS}, V_{OCS}, I_{mpps} and V_{mpps} are defined at standard conditions, STC (G_s=1000W/m^2 and T_s=25°C) and α and β are respectively the current and the voltage temperature coefficient; all the above parameters are provided by manufacturers in the cell datasheet. It is possible to note that the parameters referred to currents depends on module solar irradiance G and temperature T, while the voltage ones depends only on temperature.

The correction term $\Delta V(G)$ in (5) and (7) is necessary to account the voltage variation as a function also of solar irradiance and it is calculated as:

$$\Delta V(G) = V_{OCS} - V_{OCm}$$

where voltage V_{OCm} represents the open circuit voltage of the I-V curve translated from STC to the considered irradiance G and it defined as:

$$V_{OCm} = C_2 \cdot V_{OCS} \cdot \ln\left[1 + \frac{\left(1 - \frac{I_t}{I_{SCS}}\right)}{C_1}\right].$$

I_t is the short circuit current at irradiance G and can be written as:

$$I_t(G) = I_{SCS}(1 - \frac{G}{G_S}).$$

Azur Space triple-junction cells have been considered for the Solar Array simulations.

The SA characteristics are considered at EOL conditions to avoid degradation computation, and they are listed in Table 1.

Parameter (@ AM0)	Value
# Sections	4
P_{MPP_TOT}	250 W
V_{MPP}	42 V
I_{SC_MAX} (BOL)	2 A
V_{OC_MAX}	58 V

Table 1 : Solar Array characteristics.

4.2. Battery

The battery used in the simulations is series-parallel configured with a total capacity of 9 Ah (fading at EOL already included). EOCV and nominal current charge parameters have been set to 37.85V and 3A respectively.

The battery model already available in Simulink library has been used in the simulations.

5. SIMULATION RESULTS

In order to demonstrate the effectiveness of the parallel power management strategy, two simulations have been performed. In the first one, a power load transient shown in Fig. 6 has been accounted, together with ecl-sun & sun-ecl transitions considering the relevant variations in illumination and temperatures in addition to string failures accounted in two sections, summarized in Table 2. In particular, for the first half of the simulation the SA is supplying both the load and the battery, the latter with the current imposed by the CC-

CV algorithm. At 250s the load transient happens and the SA sections begins to operate at MPP while the battery discharges.

Parameter	Value
SA section-1 Irradiance	0 → 1000 W/m^2
SA section-2 Irradiance	0 → 1100 W/m^2
SA section-3 Irradiance	0 → 1200 W/m^2
SA section-4 Irradiance	0 → 1400 W/m^2
Temp. variations	1 °C/s
V_{batt_EOC}	37.85 V
V_{batt}	35 V (@ t=0)
I_{batt_charge}	3 A
I_{load}	2 A (flat); 30 A (pulse 60s)

Table 2: Operative conditions of the simulation.

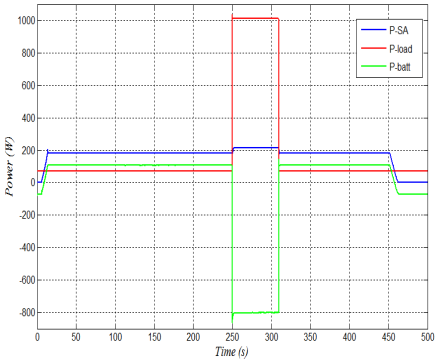

Figure 6: Power balance of the power management.

This situation lasts for 60s, after that the system returns to the previous state, so that the operating point of the SA sections moves from the MPP towards higher voltage in order to balance the power request of both the load and the battery. Figs 7 show the output SA current waveforms during the transition from discharging mode to charging mode. During charging mode, the proportional partition of the output current is being applied, maximizing the current extraction from the sections that can provide the lowest powers. In order to complete the functional verification of this system in a wide range of operative conditions. During the eclipse-sunlight transitions, the system reaches equilibrium as soon as the battery current reaches the value set as the maximum charging current, regardless of the proportional distribution. This means that the SA sections operating points ensure the energy balance between the sources, battery and load and also that the battery charge current never exceeds the imposed value. Only after a load power request that move the operating points of the SA sections to the MPP the battery current is being distributed proportionally.

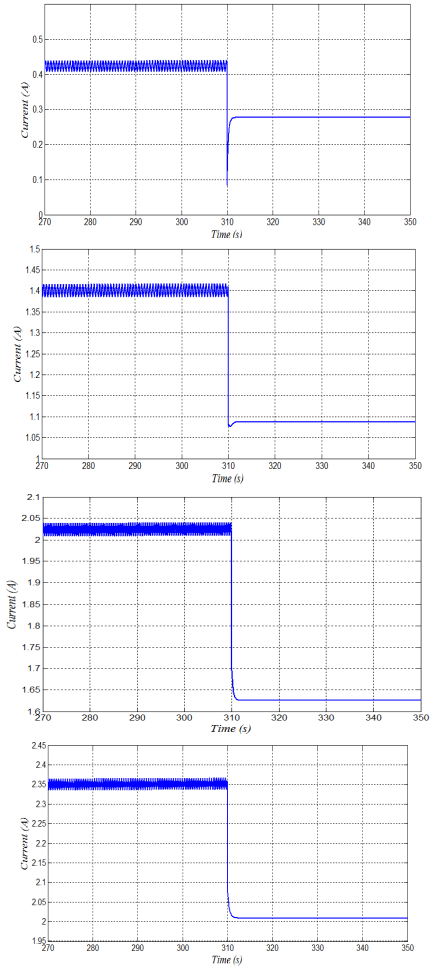

Figure 7: Output current of SA sections 1-4.

In the second simulation, the power load transient shown in Fig. 6 and the transient due to a different maximum battery charge current, starting from 5A and arriving at 1A, as illustrated in Fig. 8, have been simulated. Even in this simulation both the eclipse-sunlight and sunlight-eclipse transitions have been taken into account. The temperature and irradiance variations on the SA sections end after 180s due to the eclipse-sunlight transition. At first the maximum battery charge current is set at 5A and the total power from the SA sections allows to meet this requirement: in fact there's no need to operate at MPP at the beginning, because the maximum power is higher than the one needed for the battery charge at 5A.
This situation lasts till 85s, when the system starts to fully operate at MPP, while not satisfying anymore the 5A battery charge current condition, as the total SA power is lower than the one needed. This is because the temperature transient is not yet finished and it decreases the total SA power. Consequently, the battery current begins to be characterized by a current ripple introduced by the MPPT algorithm. At 180s even the temperature

transient ends and all SA sections reaches a steady state condition, still operating at MPP but supplying the battery with only a 3.9A charge current.
At 250s the maximum battery charge current transient happens, setting the limit at 1A. This instant represent the transition from discharging to charging operating mode, as the system exits from the MPPT phase. All the operating points of the SA sections move from the MPP to higher voltage in order to supply the battery with a lower power.
This new operative condition persists until the sunlight-eclipse transition happens and the total power becomes zero, disabling the control.
Finally, Fig. 9 shows the output currents waveforms of the DC-DC converters.

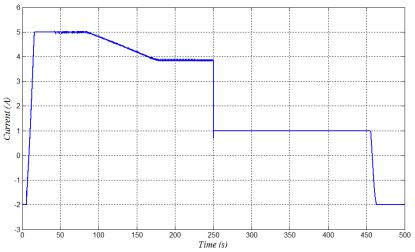

Figures 8: Battery current waveform.

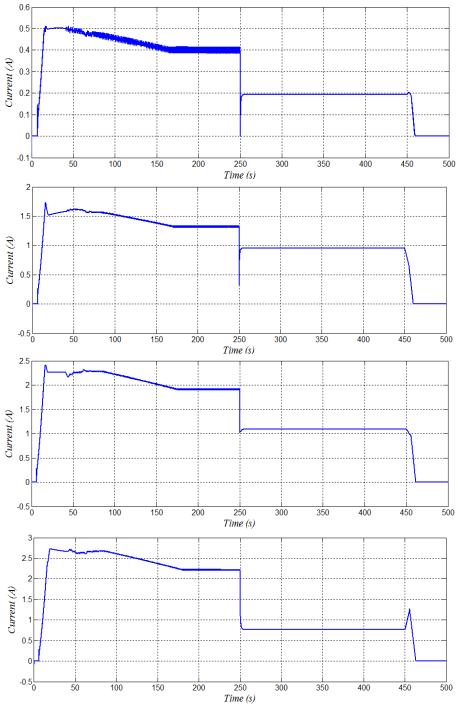

Figures 9: DC-DC converters output currents.

6. CONCLUSIONS

The proposed control strategy allows the maximization of the power extracted from every SA sections, as each one is controlled by an independent P&O MPPT algorithm. Furthermore, the developed parallel power management system allows to equally divide the stress on the power electronic components, in particular the switching devices, extending their life time and decreasing their power dissipations.

In order to validate the proposed approach, several simulation cases have been considered, accounting different operating conditions for the SA sections. The accounted simulation cases envelope the SA worst case profiles, therefore an additional improvement of the system performances and efficiency is expected. A prototype of the power module will be tested in order to validate the simulations and to verify the efficiency increasing.

7. ACKNOWLEDGMENT

This work was finalized thanks to the collaboration of C. Citriniti. This paper has been based on the result achieved in the REGIONE LAZIO Italian Project “Progettazione di un Microsatellite e Sviluppo Tecnologie Abilitanti (Cod. RL 023301).

8. REFERENCES

[1] F. Tonicello, The control problem of maximum point power tracking in power systems, Proceedings of the 7th European Space Power Conference, Stresa, Italy, 9-13 May 2005, ESA SP-589.
[2] F. Tonicello, S.Vazquez del Real, Maximum Point Power Tracker approach to a regulated bus, Proceedings of the 5th European Space Power Conference, Tarragona, Spain, 21-25 September 1998, ESA SP-416.
[3] W. Denzinger, Electrical power subsystem of Globalstar, Proceedings of the 4th European Space Power Conference, Poitiers, France, 4-8 September 1995, ESA-SP-369.
[4] L. Croci, P. Della Putta, B. Vavassori, The RADARSAT-2 Power Control Unit, Proceedings of the 6th European Space Power Conference, Porto, Portugal, 6-10 May 2002, ESA-SP-502.
[5] J. Simola, K. Savela, J. Stenberg, F.Tonicello, Maximum Power Point Regulator System, Proceedings of the 9th European Space Power Conference, Saint Raphael, France, 6-10 June 2011, ESA SP-698.
[6] Z. Varadi, V. Gorocz, J. Szabo, Power Subsystem for Small Satellites with unified operational mode controller, IEEE Conference Publishing 2011 2nd International Conference on Space Technology, Athens, Greece, 15-17 September 2011.
[7] A. Bellini, S. Bifaretti and V. Iacovone, A Simplified Model of A Photovoltaic Module, in Proc. of Applied Electronics 2009, Pilsen (Czech Republic), September 2009.
[8] W. Xiao, W.G. Dunford, and A. Capel, A novel modeling method for photovoltaic cells, IEEE Power Electronics Specialists Conference, Aachen, Germany, 2004.